NASA TECHNICAL MEMORANDUM

NASA TM X-73447

NASA TM X-73447

INVESTIGATION OF UPPER-SURFACE-BLOWING NACELLE INTEGRATION AT CRUISE SPEEDS UTILIZING POWERED ENGINE SIMULATORS

by E. T. Meleason
Lewis Research Center
Cleveland, Ohio 44135

and

O. D. Wells
McDonnell-Douglas Corporation
Long Beach, California

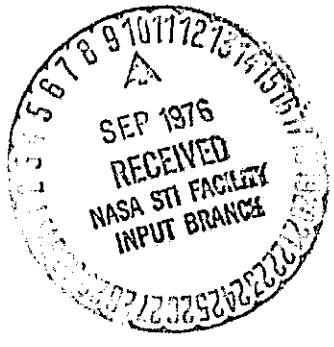

TECHNICAL PAPER to be presented at
Twelfth Propulsion Conference cosponsored
by the American Institute of Aeronautics and
Astronautics and the Society of Automotive Engineers
Palo Alto, California, July 26-29, 1976

INVESTIGATION OF UPPER-SURFACE-BLOWING NACELLE INTEGRATION AT CRUISE SPEEDS UTILIZING POWERED ENGINE SIMULATORS

by E. T. Meleason and O. D. Wells*

Lewis Research Center

E-8806

ABSTRACT

Various overwing nacelle designs were investigated on a representative four-engine short-haul aircraft configuration during a combined analytical and experimental program. Design conditions were $M_o = 0.7$ and $C_L = 0.4$. All nacelles had D-shaped nozzle exits and included a streamline-contoured design, a low boattail angle reference configuration, and a high boattail angle powered lift design. Testing was done with the design four-engine airplane configuration as well as with only inboard nacelles installed. Turbopowered engine simulators were used to provide realistic representation of nacelle flows. Performance trends are compared for the various nacelle designs. In addition, comparisons are presented between analytical and experimental pressure distributions and between flow-through and powered simulator results.

I. INTRODUCTION

Interest in upper-surface-blowing (USB) propulsion configurations has increased in recent years, particularly for short-haul missions. The over-the-wing propulsion system arrangement has been shown to provide acoustic advantages (refs. 1 and 2) along with levels of low-speed powered lift performance competitive with other powered lift systems (refs. 3 and 4). However, at cruise speeds, the placement of the propulsion nozzle and its jet directly on the wing upper surface creates a natural concern over potential interference penalties. While it appears that minimal aerodynamic interference could be achieved by contouring the nacelle to approximate local wing streamsheets (ref. 5), this approach usually conflicts with other nacelle design requirements such as good powered lift performance. At low speeds, a relatively wide, thin jet is desired for good flow turning and lift augmentation. This is usually accomplished by directing the nozzle jet onto the wing upper surface with a high boattail angle nozzle. Conversely, low boattail angles and minimal jet spreading appear desirable for low cruise drag. Previous investigators have reported (ref. 6) that compromising all the nozzle design parameters toward favorable low speed flow turning can increase the cruise drag by as much as 20 percent of total airplane drag.

This paper summarizes the results of a recent investigation of USB nacelle design tradeoffs at cruise, which was directed toward nacelles for low-pressure-ratio, high-bypass engines similar to those being developed

*McDonnell-Douglas Corporation, Long Beach, California

under NASA's QCSEE (Quiet, Clean, Short-Haul Experimental Engine) program (ref. 7). Wind tunnel tests were conducted by the NASA-Lewis Research Center with a half-span model of a representative four-engine short-haul aircraft. Configurations with only the inboard nacelles installed were also tested. Parallel analytical studies were conducted by the Douglas Aircraft Company of McDonnell-Douglas Corporation, who were also responsible for the design and fabrication of the wind tunnel model. Nacelle variations included a streamline contoured design, a low boattail angle reference configuration, and a high boattail angle powered lift design. All of the nacelles had similar D-shaped low aspect ratio nozzle exits representative of the QCSEE over-the-wing cruise nozzle geometry.

Turbopowered engine simulators were used during the test program to provide simultaneous representation of both the nacelle inlet and nozzle flows. Proper simulation of the propulsive jet is necessary since its interaction with the wing flow field can produce significant interference effects. Also, since the transonic flow field near the forward region of wings incorporating advanced airfoil sections may be sensitive to small disturbances, it was considered important to simulate the nacelle inlet and spillage flows as well. Powered engine simulators have been used successfully in other wind tunnel programs (refs. 8 to 11) and are considered to provide the most realistic representation of the complete nacelle flow environment presently available for small scale testing.

II. MODEL DESCRIPTION

Figure 1 is a photograph of the half-span model installed in the Lewis Research Center 8- by 6-foot wind tunnel. The model represented a short-haul aircraft designed for Mach 0.7 cruise, and had a cylindrical fuselage and a straight supercritical wing. The model was sized to result in a ratio of wing area to total nozzle exit area of 28.0. This value was derived from the configuration studies of reference 12 as being representative of a four engine short-haul aircraft sized to carry 150 passengers, operate from 3000 feet runways, and cruise with an engine fan pressure ratio (FPR) of 1.4. The mixed nozzle exit area required by the engine simulators resulted in a model semi-span of 27.5 inches with the aspect ratio 7.0 wing. The wing had a quarter chord sweep of 5.6 degrees, a taper ratio of 0.3, and an average section thickness of about 13.5 percent. The fuselage had a maximum diameter of 7.15 inches (13 percent of the wing span).

A typical nacelle/nozzle installation on the wing is shown in figure 2. The nozzle exits were flush on the wing upper surface and were located at 35 percent of the local wing chord. The nacelles were centered at 23 percent and 48 percent of the wing semispan, which were the standard positions used during the test. With this spacing the gap between nacelles was 1.03 nacelle diameters wide. Some limited testing was also done with the inboard nacelle located at the 28 percent semispan position.

Important nacelle geometric parameters are defined in figure 3, and figure 4 describes the three experimental nacelle configurations that were investigated. All nacelles had mixed flow convergent nozzles with similar D-shaped exit geometries. The reference nacelles, designated N_{REF}, represented a conservative cruise drag design with low boattail angles. This configuration had an external top (crownline) boattail angle of 11 degrees and an external side boattail of about 2 degrees. The streamline-contoured nacelles N_{SC}, whose design approach is described in the next paragraph, had an external top boattail angle of 6 degrees. The high angle nacelles N_{HA} represented a powered lift design from NASA's QCSEE program (ref. 7). This configuration had top centerline boattail angles of 28.5 degrees externally and 21.5 degrees internally. Because of the relatively high jet deflection angle, this configuration would not require some type of flow deflector for good low-speed powered lift performance as low angle nacelles like N_{REF} and N_{SC} would. The large sidewall boattailing of the N_{HA} nacelles (17 degrees externally and 10 degrees internally) was incorporated to minimize jet spanwise pluming at cruise.

The streamline-contoured nacelles were designed to have the nacelle contours closely match a stream sheet flowing over the top of the wing and to impose the bulk of the required boattailing in the less critical regions under the wing. The Douglas Neumann Three-Dimensional Lifting Potential Flow Computer Program (ref. 13) with the Göthert compressibility correction was used to calculate the wing-body flow field at Mach 0.7 and lift coefficient $C_L = 0.38$, and the stream sheet shapes were defined by tracing streamlines through this calculated field. Figure 5 illustrates the profile view streamlines and the resultant contoured nacelle geometry. The curvature of the streamlines in the region of the nacelles was such that the contouring would reasonably be restricted to the nozzle (aft 5.2 inches of the nacelle). The approach taken was to trace one streamline forward from the top of the nozzle exit shape (which was identical to the nozzle exit for the reference nacelle) to define the approximate position of the forward end of the nozzle. The nozzle cross-section at the forward end was also made identical to the reference nacelle, and streamlines were traced aft from this position over the wing to define design stream tubes. The design stream tubes were divided into upper and lower segments representing tubes flowing over and under the wing. The design objective was to match, as closely as possible within practical constraints, the upper stream tube profile and plan view shapes and area distributions, and the lower stream tube plan view shapes. The area distribution selected for the lower portion of the nozzle and under wing fairing was intended to violate the design stream tube requirements in relatively insensitive regions (favorable pressure gradient regions) of the flow field. The convergence of the internal ducting for the contoured nacelle was set equal to that of the reference nacelle over the last inch of the nozzle. This convergence, along with practical structural constraints, produced modest boattail angles relative to the design stream tube near the nozzle exit.

III. POWERED SIMULATOR CONSIDERATIONS

The turbopowered engine simulators that were used in this investigation were Tech Development, Inc., model No. 800's (fig. 6). An air-driven, two-stage turbine powers a two-stage fan. At design conditions the fan develops a total pressure ratio of about 1.66 at 85,000 rpm. The diameter of the fan is 2.80 inches.

Calibration

Prior to the wind tunnel test, the complete nacelles with engine simulators were calibrated statically at the Douglas Aircraft Company Aerophysics Lab in the facility shown schematically in figure 7. The facility exhausted to atmosphere, and proper values of nozzle pressure ratio were achieved by pressurizing the inlet air supply. A plate simulating the wing upper surface contour was attached to the nozzle through a separate balance, and its drag contribution was deleted. Nozzle axial thrust was calibrated as a function of nozzle pressure ratio for each simulator/nozzle combination. At the same time, fan airflow was calibrated as a function of inlet static to total pressure ratio, using a sonic flow nozzle to measure the airflow. The simulator turbine drive airflow, which constituted about 25 percent of the nozzle exhaust flow, was measured with a sharp-edge orifice for both the calibration and wind-tunnel installations.

The calibration determined a nozzle velocity coefficient C_V which related measured thrust to the measured weightflow values. The velocity coefficient is defined as:

$$C_V = \frac{Fg_S}{Fg_i} = \frac{Fg_S}{\frac{W_F}{g} V_{F_i} + \frac{W_T}{g} V_{T_i}}$$

where,

Fg_S = measured gross thrust at static conditions

Fg_i = ideal gross thrust

W_F, W_T are measured fan and turbine weight flow rates

V_{F_i}, V_{T_i} are the ideal values of fan and turbine flow velocities after expansion to ambient pressures. These ideal velocities are computed from measured flow properties.

g = gravitational constant

Some typical calibration results are shown in figure 8. The total scatter in experimental velocity coefficient values is less than $\pm$ 0.5 percent

and compares well with an estimated uncertainty based on instrumentation accuracies and influence coefficients.

These nozzle velocity coefficients are used to define net thrust of the powered simulators in the wind tunnel through the relation:

$$F_{NET} = C_V \cdot Fg_i + (p_L - p_o)A_E - \frac{W_F}{g} V_o$$

where,

C_V is evaluated at the local nozzle pressure ratio, using an average of measured values of local external pressure at the nozzle exit, p_L.

p_o = free stream static pressure

A_E = nozzle exit area

V_o = free stream velocity

The term $(W_F/g)V_o$ is the ram drag of the fan flow.

Drag Definition

Cruise drag results are presented in terms of a drag penalty parameter which is illustrated in figure 9. This drag penalty is the difference between the total configuration drag with nacelles installed minus the separate isolated drags of the nacelle and clean wing configuration. The measured drag of the complete model configuration with powered simulator installed consisted of balance forces corrected for the calibrated net thrust of the powered nacelle. The isolated nacelle drag was an estimate, based on nacelle fineness ratio, for a well-behaved axisymmetric nacelle with no separation. This estimate was made at free stream Mach number, and in the case of the streamline-contoured nacelle N_{SC}, included the additional external drag of the lower wing surface fairing. The drag of the basic clean wing configuration without nacelles was measured. This drag was evaluated at values of Mach number and lift coefficient identical to those of the nacelle-on configuration. An estimate was made of the skin friction drag for that portion of the wing covered by the nacelle, and this increment was subtracted from the measured clean wing drag. When the separate isolated drags of the nacelle and clean wing are subtracted from the total configuration drag, anything left over is considered a drag penalty. Included in this drag penalty parameter would be any unfavorable interference effects, any increased nacelle pressure drag due to flow separation, and the scrubbing drag of the jet flow on the wing upper surface.

Power Effects

Figure 10 is a direct comparison between powered simulator drag results and flow-through nacelle drag results for a four-engine configuration at Mach 0.7. The experimental nacelles were slightly modified versions of N_{HA} which had small external fairings added to the nozzle boattail to represent an alternate QCSEE nozzle design. These nacelles were used for this comparison in order to present the most extensive range of data available. The parameter $(\Delta C_D)_{POWER}$ is the difference in configuration drag coefficient (powered minus flow-through). Non-zero values of this parameter indicate an effect of power, and the data shows that this effect is indeed present and varies with both simulator fan pressure ratio and airplane lift coefficient C_L. For reference, a drag increment is indicated equivalent to 5 percent of cruise net thrust (or airplane drag) at design conditions (four-engine configuration, $M_0 = 0.7$, $C_L = 0.4$, FPR = 1.37), and it is seen that the power effect can approach this value. Note that as fan pressure ratio is reduced toward the flow-through reference value (FPR = 1.0) the power effect data all tends to come together and approach zero.

In figure 11 power effect is compared for the three nacelle designs at Mach 0.7 and $C_L = 0.4$, this time with only inboard nacelles installed. The power effect is seen to also be a function of nacelle design. Note that the effect of the jet becomes more favorable in going from N_{SC}, the nacelle with the lowest jet deflection, to N_{HA}, which has the highest jet deflection.

IV. TEST RESULTS

Inboard Nacelles Only

Although all nacelles were sized to correspond to a four-engine airplane configuration, some testing was conducted with only inboard nacelles installed to evaluate the various designs without any nacelle-to-nacelle interference effects present. Experimental drag penalties are shown in figure 12 for the inboard nacelle configuration (single nacelle installed on the half-span wind tunnel model). The powered nacelles were located at the 23 percent semispan inboard position and data are shown for a fan pressure ratio of 1.37 and a lift coefficient of 0.4, corresponding to Mach 0.7 cruise design conditions. At these conditions the nozzle pressure ratio was about 1.9 based on free stream static pressure. Local nozzle pressure ratio was about 2.2 for N_{REF} and N_{HA}, and slightly higher for N_{SC}.

The various nacelles are seen to exhibit markedly different drag behavior with Mach number. The reference nacelle shows a small, nearly constant drag penalty over most of the Mach number range but develops a strong favorable interference effect at the higher Mach numbers where the wing is well into drag rise. The streamline-contoured nacelle shows a negligible

penalty at the lower Mach numbers and a sharp increase as the wing enters drag rise. Drag penalty associated with the high-angle nacelle exhibits a steady increase with Mach number.

At the design Mach number of 0.70, the reference nacelle and the streamline-contoured nacelle both show drag penalties in the range of 1.0 to 1.5 percent of net thrust or airplane drag. A significant part of this penalty is probably associated with the additional scrubbing drag of the jet on the wing upper surface. These results indicate that the reference nacelle has good drag characteristics and, at design, no appreciable advantage is gained by streamline-contouring the nacelle. The high boattail angle nacelle N_{HA} exhibited a considerably higher drag penalty at Mach 0.7, equal to about 5 percent of net thrust.

Figures 13 and 14 compare wing surface pressures just outboard of the nacelle for the various configurations at Mach 0.7. In figure 13, pressures measured with the streamline-contoured nacelle are compared to clean wing pressures. Good agreement is seen, with a slight aft movement of the wing shock indicated. Note that the airplane lift coefficient was only slightly affected by the installation of the powered streamline-contoured nacelle at angle of attack α = 1.0 degrees.

In figure 14, the same wing pressures are compared for the reference and high angle nacelles. With these configurations, there was a significant effect of the powered nacelle installation on airplane lift, as indicated by lift coefficients near 0.4 being obtained at a reduced angle of attack (0.5 degrees compared to 1.0 degrees for the clean wing). With the high angle nacelle, the region of supercritical flow on the wing upper surface was more extensive as the wing shock was moved aft toward the nozzle exit. With the reference nacelle, the wing shock was slightly forward of the clean wing position.

Top centerline boattail pressures for the three nacelles at the Mach 0.7 design conditions are shown on figure 15. The reference nacelle, which had the most forward wing shock position, had nearly constant velocity subcritical flow over the boattail. The other two nacelles, where the wing shock was seen to be further aft, had similar higher velocity flow distributions which reached near sonic levels. With the streamline-contoured nacelle with its negligible aft-facing boattail projected area, these high velocity flows and resultant low pressures would not cause a significant drag penalty. However, the high angle boattail nacelle with its large boattail projected area would see a significant interference drag penalty from this effect.

At Mach 0.76, where the wing is well into drag rise, the drag results of figure 12 showed that the reference nacelle installation was beginning to exhibit a favorable interference effect while the other two nacelles were showing high drag penalties. Figure 16 compares wing surface pressures at these conditions for the reference nacelle and the streamline-contoured nacelle; the instrumentation location is again just outboard of the nozzle

at 53 percent semispan. Wing pressures with the streamline-contoured nacelle again closely match the clean wing data, with the wing shock well aft of the nozzle exit. With the reference nacelle installation, where equivalent lift is generated at a reduced angle of attack, the wing shock is ahead of the nozzle exit and well ahead of the clean wing shock position. The reference nacelle thus acts to hold the wing shock upstream of the nozzle exit as the wing enters drag rise, while the streamline-contoured nacelle does not. A consequence of this is that the streamline-contoured nacelle is exhausting into a much lower pressure field compared to the reference nacelle. Additional wing pressure measurements downstream of the nacelle centerline showed strong pressure fluctuations in the overexpanded jet flow behind the streamline-contoured nacelle, which doubtless contributes to the higher drag penalties seen with this nacelle at these conditions.

Four-Engine Configurations

In figure 17, experimental drag penalties are presented for the reference nacelle and high angle nacelle for the four-engine airplane configuration (two nacelles on the half-span model). The powered nacelles were located at 23 percent and 48 percent of semispan, and data are again shown at the design fan pressure ratio (FPR = 1.37) and lift coefficient (C_L = 0.4). Again, relatively low drag penalties are seen for the reference nacelles, with considerably higher drag penalties for the high boattail angle nacelles. At the cruise Mach number of 0.7, the reference nacelle penalty was less than 3 percent of design net thrust, or about twice the level observed with only inboard nacelles installed (fig. 12). With the high angle nacelles, the drag penalty at Mach 0.7 was about 12 percent of net thrust. This was more than twice the penalty with inboard nacelles only from figure 12, which would be about 9 percent. Wing surface pressures between the nacelles (fig. 18) again show a more extensive region of supercritical flow with the high angle nacelles. The terminal shocks on the wing upper surface are well defined, and the one associated with the high angle nacelles is appreciably stronger. Comparison of the N_{HA} pressure distribution with the inboard nacelle only case previously seen in figure 14 shows that the presence of the outboard nacelle produced a significant acceleration of the supercritical flow in the channel region. This interference effect between nacelles probably accounts for the additional drag penalty (over twice the level with inboard nacelles only) seen with this design.

Spanwise Nacelle Variations

Drag measurements were made with an alternate four-engine nacelle arrangement, where the inboard nacelle was moved from 23 percent semispan to 28 percent. This reduced the gap between nacelles by about 40 percent, from 1.03 nacelle diameters to 0.63. The reference nacelles were used for this variation, and the results are shown on figure 19. At the design lift coefficient of 0.4, only a slight drag penalty increase is seen at the higher Mach numbers with the reduced spacing. At a lift coefficient of 0.5 a more

pronounced increase is seen (up to about 5 percent of net thrust), but again only at Mach numbers beyond design.

The drag variation with spanwise position for a single nacelle on the half-span model is shown in figure 20 for the flow-through reference nacelles. Also shown for comparison are data with both nacelles installed. Moving the nacelle outboard from the 23 percent semispan position to the 48 percent position generally resulted in a small drag reduction of a few counts. The sum of the two drags obtained with single nacelles was in most cases quite close to the drag level seen with both nacelles installed, indicating that mutual interference between nacelles is generally negligible for this configuration.

Analytical Comparisons

Analytical estimates of the pressure distributions on the configuration were made using the Douglas Neumann program (ref. 13). Mach number effects were included by using the Göthert compressibility correction. The geometry included the estimated boundary layer thickness on the wing. The nacelle exhaust and intake flows were represented as solid bodies. For a nozzle total pressure to freestream total pressure ratio (NPR) of 1.0, these solid bodies were obtained by tracing streamlines forward from the highlight location and aft from the nozzle location in the wing-body flow field.

The analytical estimates are compared to the data on figures 21 and 22. Except for the nacelle-off data being generally more negative (lower pressures) than the estimate the incremental trends due to the nacelle installation are predicted fairly well. The magnitude of the increments due to nacelle installation are generally larger than predicted, producing better agreement with the nacelles on than off. The significant supercritical region between the nacelles contributes to the analytical-experimental disagreement in this area.

The effects of power were estimated analytically using the Neumann program combined with an estimated jet shape at a NPR of 1.4. The jet shape was obtained using the Method of Characteristics to solve for a jet boundary that matched the boundary conditions imposed by the wing solid surface and by the pressure on the jet surface obtained from the Neumann off-body flow field in the region of the jet. The trajectory of the jet aft of the wing trailing edge was obtained by solving for the shape of a thin jet issuing from the wing trailing edge in the presence of the wing, using the Douglas Elementary Vortex Distribution (EVD) calculation procedure (ref. 14).

The results of the analysis for 38 percent semispan are shown in figure 23 using the outboard nacelle location. The overall character of the pressure distribution is not greatly affected by the jet. Test data was not obtained for the outboard nacelle location but was available for an inboard nacelle location at a slightly lower pressure ratio and these results are

shown on figure 24. A comparison between the test data and the analysis indicates that the experimental incremental effects due to the jet are closely predicted by the analysis except near ten percent chord on the upper surface where a supercritical flow region exists.

VI. CONCLUSIONS

1. With only the inboard nacelles of the four-engine airplane configuration installed, USB nacelles with moderate boattail angles (N_{REF} and N_{SC}) exhibited small cruise drag penalties of 1 to 1.5 percent of net thrust (3 to 5 airplane drag counts) at Mach 0.7 design conditions. Drag penalty with the non-contoured reference nacelle was essentially equivalent to that of the streamline-contoured nacelle at the design conditions.

2. A high boattail angle nacelle (N_{HA}) designed for powered lift showed a significantly larger drag penalty, about 5 percent of net thrust or 15 drag counts. This penalty was associated with low pressures over the nozzle boattail and an enlarged region of supercritical flow on the wing upper surface as the wing shock was moved aft from its clean wing position.

3. With a four-engine configuration, drag penalty at Mach 0.7 with the reference nacelles was about twice the level observed with only inboard nacelles installed. For N_{HA} nacelles, an additional penalty was present and was associated with additional supercritical flow acceleration in the channel between nacelles.

4. The effect of power on the experimental results varied with fan pressure ratio, lift coefficient, nozzle design, and Mach number. At Mach 0.7, flow-through and powered results differed by more than 5 percent of design net thrust.

5. Reducing the spacing between the N_{REF} nacelles from 1.03 nacelle diameters to 0.63 nacelle diameters produced a slight additional drag penalty.

6. There was little effect of spanwise nacelle position on drag for the two-engine configuration with flow-through reference nacelles. Spanwise position was varied from 23 percent semispan to 48 percent. Drag at the outboard nacelle position was slightly less than inboard.

7. Incremental effects of nacelle installation and power on wing pressure distributions were reasonably well predicted by analytical techniques.

REFERENCES

1. von Glahn, U., Reshotko, M., and Dorsch, R., "Acoustic Results Obtained with Upper-Surface-Blowing Lift-Augmentation Systems," TM X-68159, 1972, NASA.

2. Dorsch, R., "Externally Blown Flap Noise Research," TM X-71541, 1974, NASA.

3. Johnson, J. L., Jr., and Phelps, A. E., III; "Low-Speed Aerodynamics of the Upper-Surface Blown Jet Flap," SAE paper 740470, Dallas, Tex., 1974.

4. Wimpress, J. K., "Upper Surface Blowing Technology as Applied to the YC-14 Airplane," SAE paper 730916, Los Angeles, Calif., 1973

5. Gillette, W. B., et al., "Upper-Surface Blowing Nacelle Design Study for a Swept Wing Airplane at Cruise Conditions," CR-2427, 1974, NASA.

6. Skavdahl, H., Wang, T., and Hirt, W. J., "Nozzle Development for the Upper-Surface Blown Jet Flap on the YC-14 Airplane," SAE paper 740469, Dallas, Tex., 1974.

7. Ciepluch, C. C., "QCSEE Program," Aeronautical Propulsion, SP-381, 1975, NASA, pp. 65-80.

8. Welge, H. R. and Ongarato, J. R., "Powered Engine Simulator Procedures and Experience for the DC-10 Wing Engine," Journal of Aircraft, vol 8, July 1971, pp. 523-529.

9. Motycka, D. L., Sabato, V. J., and Anderson, L. Q., "The Use of a Powered Model for Subsonic Nacelle Optimization," ASME paper 72-GT-14, San Fransico, Calif., 1972.

10. Decher, R. and Tegeler, D. C., "High Accuracy Force Accounting Procedures for Turbopowered Simulator Testing," AIAA paper 75-1324, Anaheim, Calif., 1975.

11. Steffen, F. W., "Cruise Performance of an Isolated 1.15 Pressure Ratio Turbofan Propulsion System Simulator at Mach numbers from 0.6 to 0.85," TM X-3064, 1974, NASA.

12. "Study of Quiet Turbofan STOL Aircraft for Short-Haul Transportation Volume 2: Aircraft," MDC-J4371-Vol.-2, June 1973, Douglas Aircraft Co., Inc., Long Beach, Calif.; also CR-114607, NASA.

13. Friedman, D. M., "A Three-Dimensional Lifting Potential Flow Program," MDC-J6182, Sept. 1974, Douglas Aircraft Co., Inc., Long Beach, Calif. (Proprietary restricted distribution).

14. Lopez, M. L., Shen, C. C., and Wasson, N. F., "A Theoretical Method for Calculating the Aerodynamic Characteristics of Arbitrary Jet Flap Wings Volume 1: The Elementary Vortex Distribution Jet-Wing Lifting Surface Theory," MDC-J5519-01-Vol.-1, May 1973, Douglas Aircraft Co., Inc., Long Beach, Calif.

Figure 1. - U. S. B. propulsion integration model in wind tunnel.

Figure 2. - Typical nacelle installation.

β_{TOP} = TOP ℄ BOATTAIL ANGLE (EXTERNAL)
δ_{TOP} = TOP ℄ DEFLECTION ANGLE (INTERNAL)
φ = SIDEWALL EXTENSION ANGLE
β_{SIDE} = SIDE BOATTAIL ANGLE (EXTERNAL)
δ_{SIDE} = SIDE DEFLECTION ANGLE (INTERNAL)
w = WIDTH
h = HEIGHT

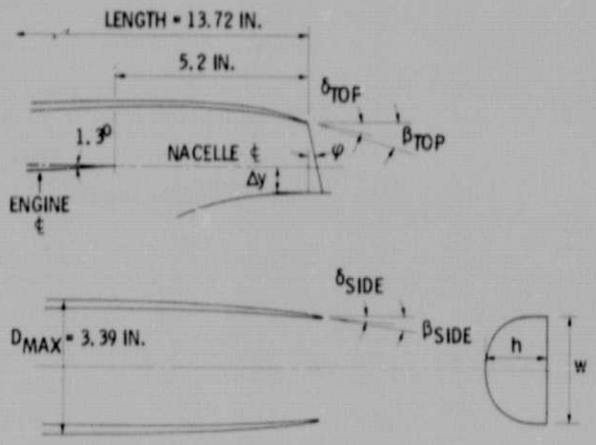

Figure 3. - Definition of nacelle parameters.

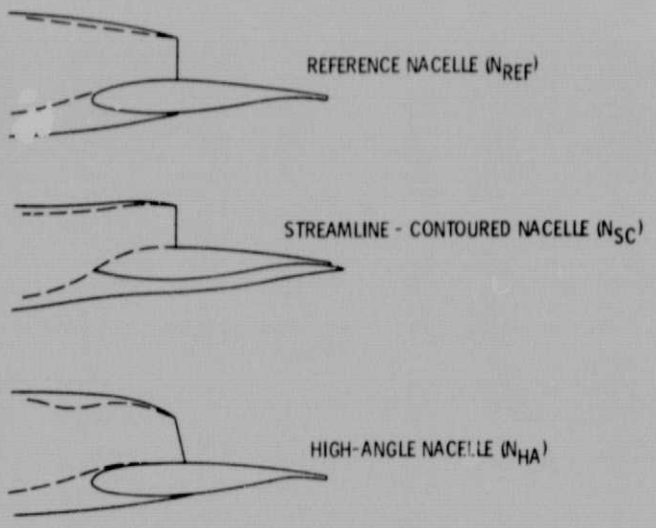

	β_{TOP}	δ_{TOP}	β_{SIDE}	δ_{SIDE}	φ	w/h	$\Delta Y/D_{MAX}$
N_{REF}	11.0°	4.0°	2.0°	0.0°	0°	2.17	0.105
N_{SC}	6.0°	1.0°	2.5° IB 7.5° OB	-0.5° IB 4.5° OB	0°	2.17	-0.139
N_{HA}	28.5°	21.5°	17.0°	10.0°	15°	1.90	0.161

Figure 4. - Experimental nacelle configurations.

E-6806

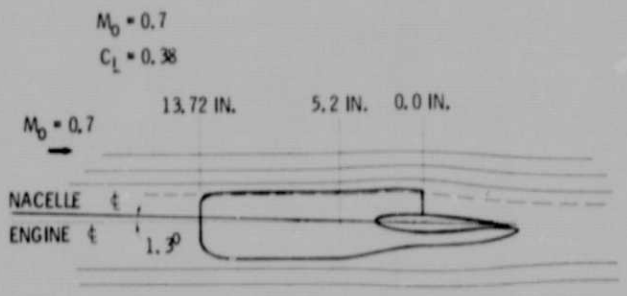

Figure 5. - Streamline contoured nacelle, profile view.

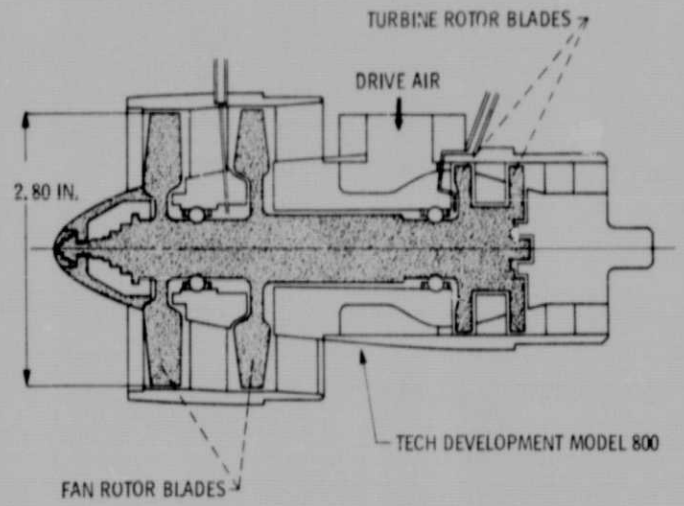

NOTE: SHADED REGION DENOTES ROTATING HARDWARE

Figure 6. - Turbopowered engine simulator.

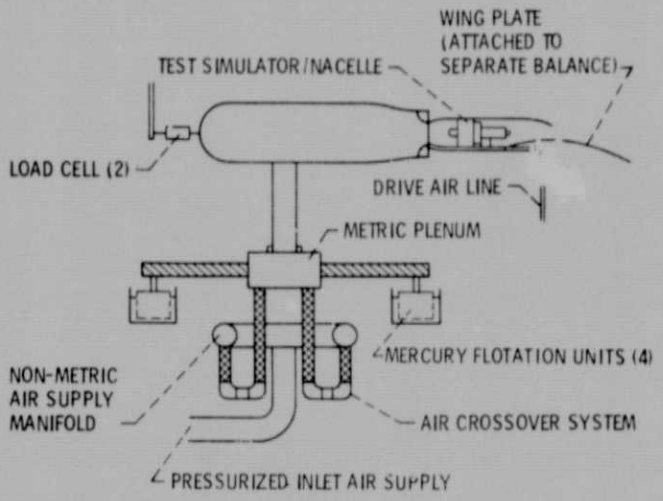

Figure 7. - USB nacelle/simulator static calibration stand.

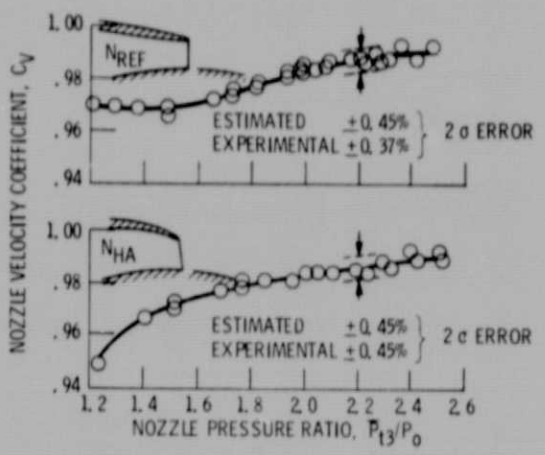

Figure 8. - Static calibration results.

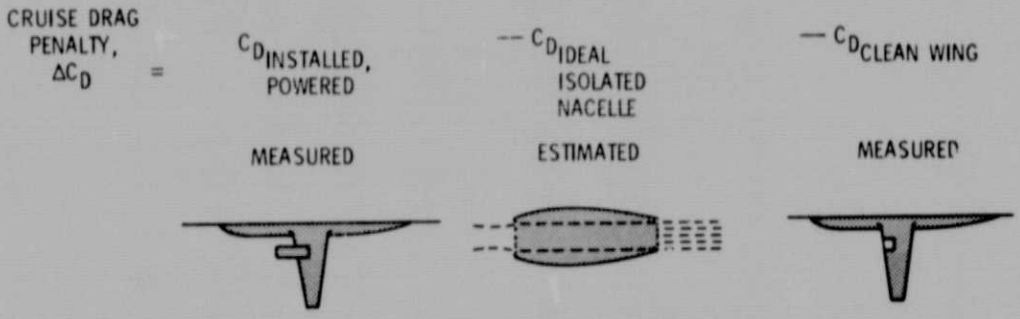

Figure 9. - Drag definition.

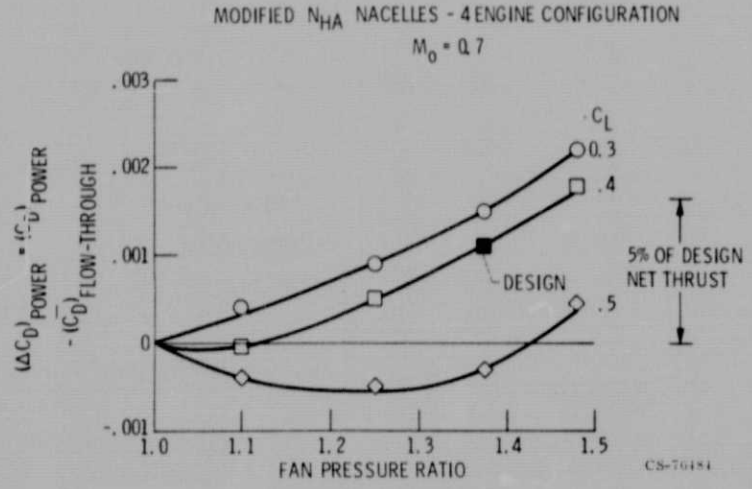

Figure 10. - Power effect.

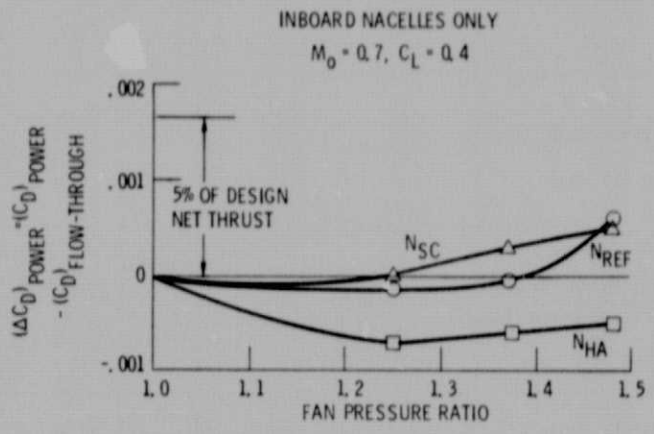

Figure 11. - Power effect for various nacelle configurations.

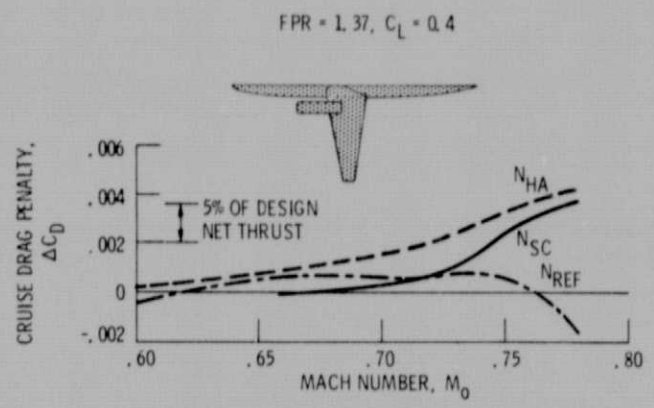

Figure 12. - Drag results with only inboard nacelles installed.

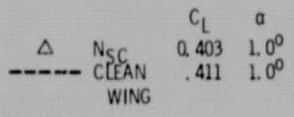

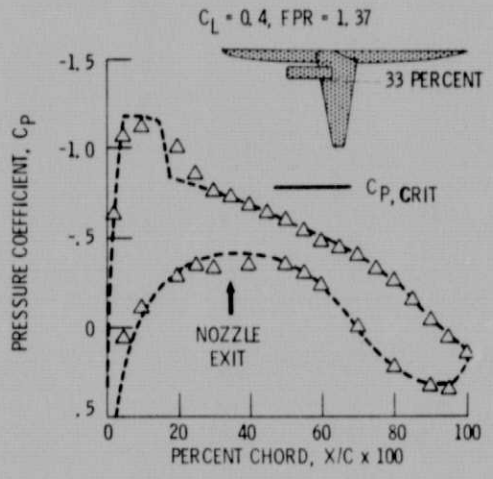

Figure 13. - Wing pressures alongside N_{SC} nacelle at Mach 0.7.

E-6806

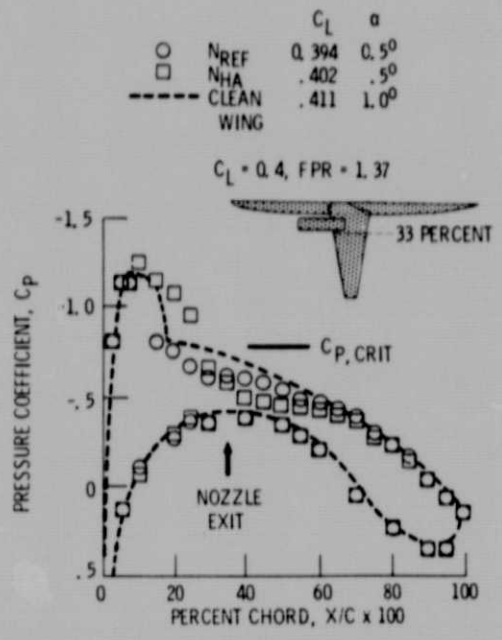

Figure 14. - Wing pressures alongside N_{REF} and N_{HA} nacelles at Mach 0.7.

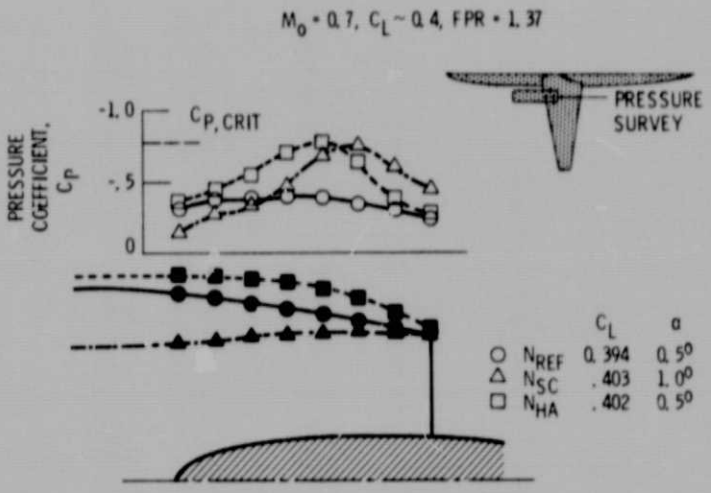

Figure 15. - Comparison of external boattail pressures.

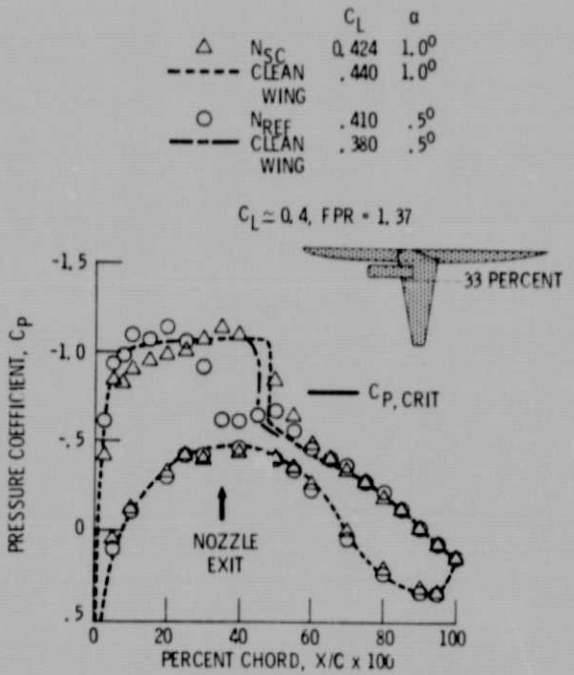

Figure 16. - Wing pressures alongside N_{SC} and N_{REF} nacelles at Mach 0.76.

E-8306

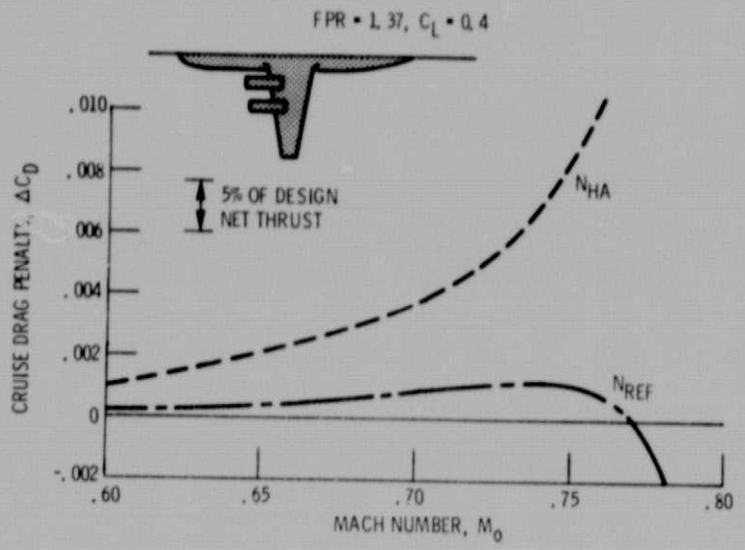

Figure 17. - Drag results with four-engine configuration.

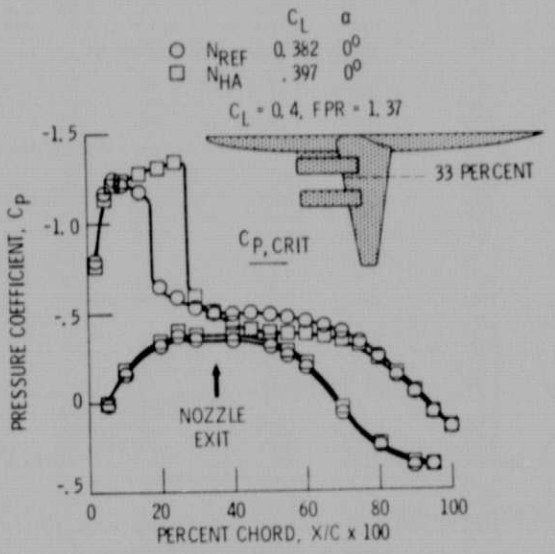

Figure 18. - Wing pressures between nacelles at Mach 0.7.

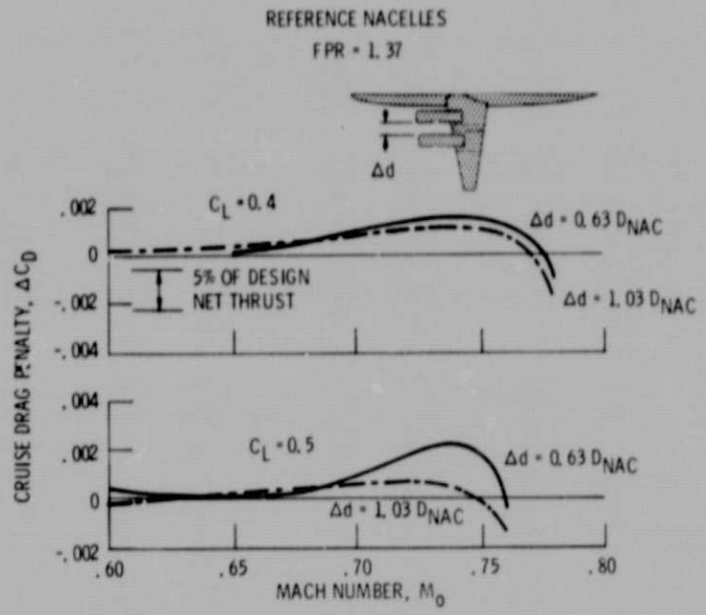

Figure 19. - Effect of nacelle spacing.

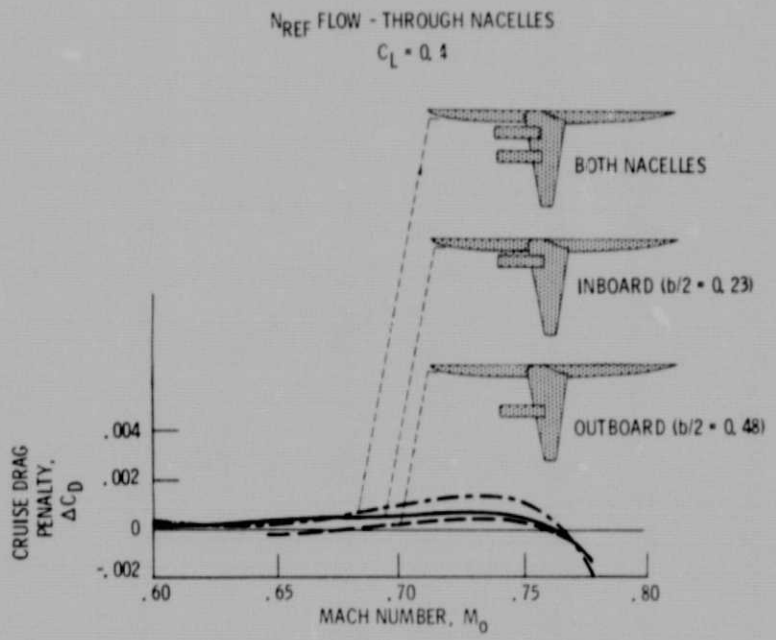

Figure 20. - Effect of spanwise position.

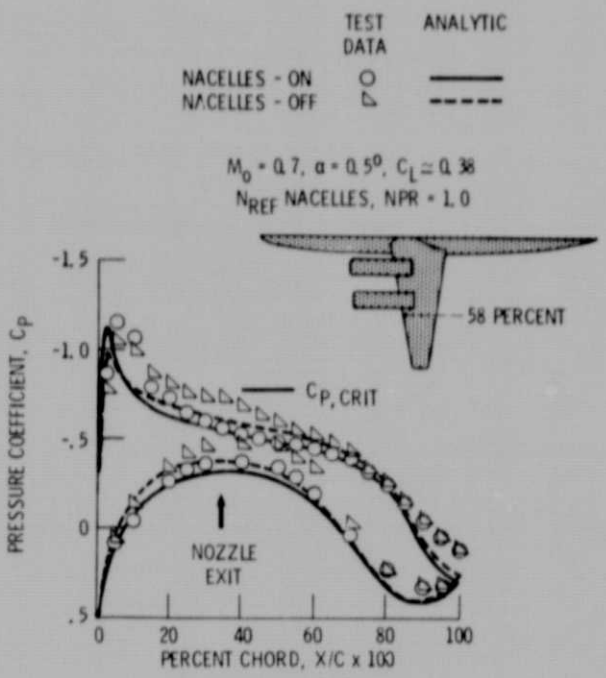

Figure 21. - Comparison of analytical and experimental wing pressures outboard of nacelles - nacelles on vs nacelles off.

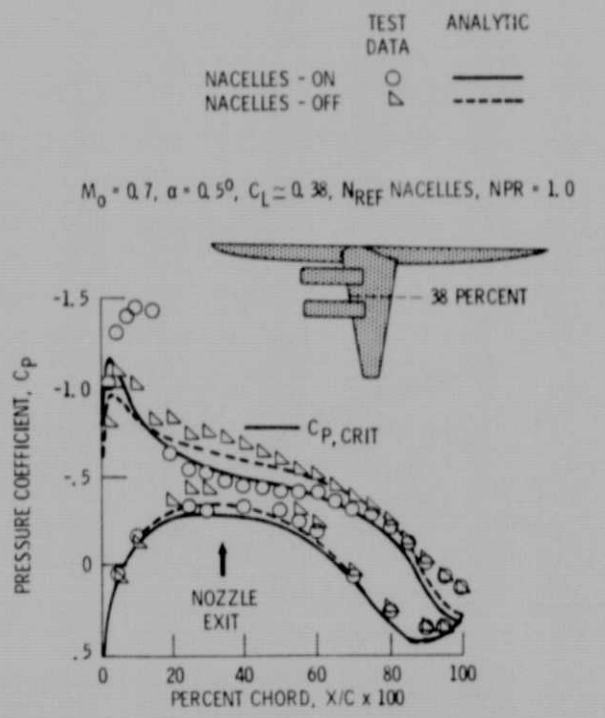

Figure 22. - Comparison of analytical and experimental wing pressures between nacelles - nacelles on vs nacelles off.

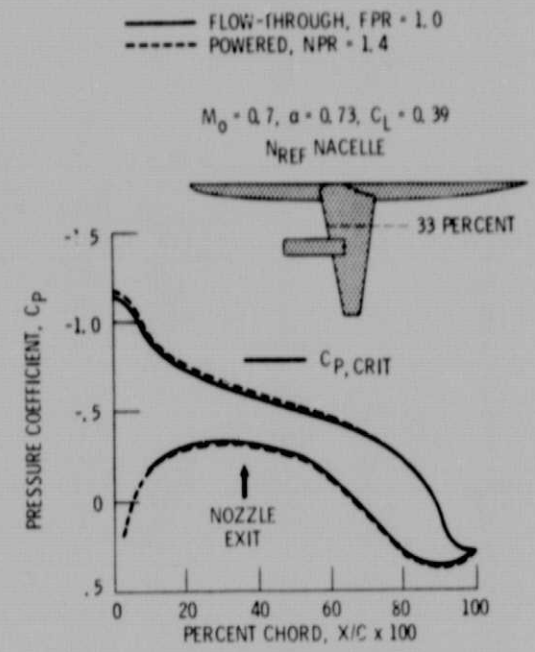

Figure 23. - Comparison of analytical wing pressures with and without power.

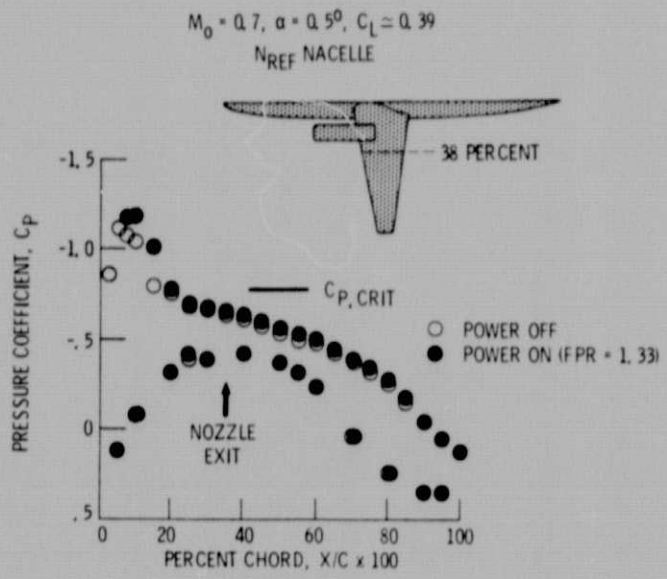

Figure 24. - Comparison of experimental wing pressures with and without power.